JPEDAV (2005) 26:539-546
DOI: 10.1361/154770305X66691
1547-7037/$19.00 ©ASM International

The Role of Grain Boundary Diffusion in Initial Selective Oxidation Kinetics of a Manganese-Aluminum TRIP Steel

Casper Thorning and Seetharaman Sridhar

(Submitted July 20, 2005)

Confocal scanning laser microscopy (CSLM) was used in real-time observation of alloy element oxidation of a manganese/aluminum transformation induced plasticity (TRIP) steel. CSLM images reveal a marked role of grain boundaries in the overall initial oxidation kinetics of the alloy and consequently in the morphology of the initial surface oxide. Changing the grain size and the oxidation temperature results in a change in the overall kinetics of selective oxidation and in the importance of oxidation at grain boundaries, respectively. Electron backscattered diffraction mapping was used to characterize the grain boundaries intersecting the surface over an area of the alloy. Subsequent CSLM observation of selective oxidation over the same area allowed quantification of oxidation kinetics as a function of individual grain boundary misorientation.

1. Introduction

The exposure of an alloy to an atmosphere containing oxygen can generally be illustrated as in Fig. 1. The alloy consists of a base metal, (A) with one or more alloying elements (B and C) in solid solution. The alloy is in contact with an atmosphere with an oxygen potential, pO_2. In the case that the pO_2 is high enough for oxides of all the elements A, B, and C to form, the following mechanisms of formation of oxide compounds are possible.

The base metal, A, is in direct contact with the oxidizing gas, and an oxide compound A_xO_y forms on the surface of the alloy. The rate-limiting step is initially the supply of oxygen from the surrounding atmosphere. As shall be discussed later, this supply may be controlled by the oxidation of B or C if any of these has a higher affinity for oxygen than A does. When the oxide of A has grown sufficiently to form a coherent layer across the surface of the alloy, thus separating the unreacted A and oxygen, diffusion of these species through the oxide layer becomes rate limiting to further growth.

Alloying elements B and C may form oxides on reaction with oxygen, either externally at the surface of the alloy (B in Fig. 1) or internally, below the original surface of the alloy (C in Fig. 1). Whether an alloying element oxidizes internally or externally depends on: The pO_2 of the oxidizing gas, the concentration of the alloying element in the alloy, the diffusivity of oxygen in the alloy, and the diffusivity of the alloying element in the alloy.

If we regard alloying element B, the criterion for external oxidation can be given as in Eq 1.[1]

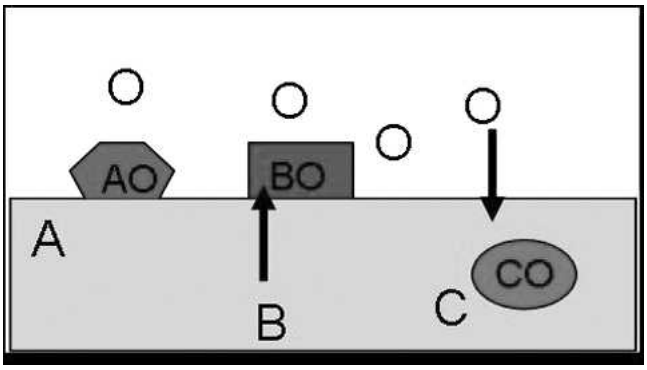

Fig. 1 Schematic of alloys oxidation

$$N_B^{(0)} > \left[\frac{\pi g^*}{2v} N_O^{(S)} \frac{D_O V_m}{D_B V_{OX}}\right] \quad \text{(Eq 1)}$$

Here, $N_B^{(0)}$ is the concentration of B in the alloy, $N_O^{(S)}$ is the solubility of oxygen in base metal A, D_O and D_B are the diffusivities of oxygen and B in A, respectively, and g^* is a critical value of the volume fraction of oxide:

$$g = f\left(\frac{V_{OX}}{V_m}\right) \quad \text{(Eq 2)}$$

where V_m is the molar fraction of oxide BO_v in the internally oxidized zone. $N_O^{(S)}$ is directly related to pO_2 in the oxidizing atmosphere.

From Eq 1, it can be predicted how the exposure conditions affect the transition from internal to external oxidation. External oxidation may be promoted by increasing the concentration of the oxidizing element, $N_B^{(0)}$, increasing the diffusivity of the oxidizing element, D_B, and/or lowering the pO_2 (lowering $N_O^{(S)}$). The former two measures increase the

This article is a revised version of the paper printed in the *Proceedings of the First International Conference on Diffusion in Solids and Liquids—DSL-2005*, Aveiro, Portugal, July 6-8, 2005, Andreas Öchsner, José Grácio and Frédéric Barlat, eds., University of Aveiro, 2005.

Casper Thorning and **Seetharaman Sridhar,** Department of Materials Science and Engineering, Carnegie Mellon University, Pittsburgh, PA 15213. Contact e-mail: ctmr@andrew.cmu.edu.

outward flux of B, whereas the latter reduces the inward flux of oxygen.

Increasing the D_B was proposed to be accomplished mainly by reducing the grain size of the alloy, thus increasing the high-diffusion grain boundary area. It is observed that the substrate microstructure has a significant influence on selective oxidation kinetics.[2-7] In an interesting way, two opposite trends in this correlation are observed. In pure metals, oxidation rates increased in cold-worked specimens, the increase being attributed to dislocations acting as vacancy sinks. In iron (Fe)-based alloys containing chrominum (Cr), a decreased oxide growth rate is observed with decreasing grain size when oxidized at high temperature in atmospheres oxidizing both Fe and Cr.[3-6] An explanation for this observation is that the increased grain boundary area in the fine-grained samples, acting as high-diffusion paths, offers an increased supply of chromium (Cr) to the oxidation front. A protective layer of Cr oxide is then established more rapidly on the finer-grained samples, reducing the overall oxidation rate through suppression of the oxidation of Fe. An identical conclusion was drawn from similar experiments on Ni-Cr-Al-Y alloys.[2]

Several careful investigations have shown a heterogeneous oxidation behavior of alloys, with oxidation at the grain boundaries of different chemistry and kinetics other than that of the grain interior surfaces, leading to modifications of Eq 1 to accommodate the greater D_B at grain boundaries.[8] One obstacle to such an analysis is the lack of data on the diffusivity of substitutional solutes in grain boundaries. As a further complication, solute diffusivity along grain boundaries is observed to be strongly dependent on the character of the grain boundary. Data that correlate the grain boundary character and diffusivity have been reviewed by Sutton and Balluffi[9] and have been collected mainly for special types of grain boundaries, such as pure tilt or pure twist boundaries, where the atomic structure can be more readily understood. Grain boundary diffusivity is observed to decrease markedly at coincidence site lattice boundaries in fcc metals, where grain boundary energy and grain boundary free volume are low. However, diffusivity data are limited for random boundaries and for lattices other than fcc.

This paper is part of a study in which the role of grain boundaries on TRIP steel oxidation kinetics during heating and isothermal conditions is being investigated. The role of boundary is expected to change during heating as austenite formation and grain migration take place. This paper focuses on the oxidation behavior at lower temperatures where the microstructure is stable. The purpose of the present investigation is to provide in situ observation of the relative kinetics of oxidation at grain boundaries and grain interior surfaces as a function of temperature and grain size to probe the mechanisms mentioned above. Further, an attempt is made to correlate the oxidation rate, as a measure of diffusivity, to grain boundary misorientation at a wide range of grain boundaries. Finally, a suggestion is given as to how the methods used in the current study may be expanded to correlate grain boundary diffusivity to the full characteristics of individual grain boundaries.

2. Experimental

2.1 Material Composition and History

A TRIP steel with the composition 0.144 wt.% carbon (C), 1.81 wt.% manganese (Mn), 0.069 wt.% silicon (Si), and 1.57 wt.% aluminum (Al) was melted in a vacuum furnace and cast into 5 × 12 in. = 127 × 305 mm steel molds. The steel was hot rolled in seven passes at 1280 °C down to a 1 in. thickness with the final pass temperature being about 900 °C. Subsequent to hot rolling the sample was reduced in thickness by 25% by milling to avoid surface segregation effects. The steel was then cold rolled to a final thickness of 1.6 mm. The grain size of the specimens in this condition was approximately 5 μm, and these specimens are called fine-grained throughout. To study the effect of grain size some specimens were annealed in H_2 at 1050 °C for 2 h followed by furnace cooling, resulting in a coarsening of the grain size to approximately 20 μm. These specimens are referred to as coarse-grained.

2.2 Experimental Procedures

Sample surface crystallography was measured in the coarse-grained samples by electron backscattered diffraction (EBSD) at room temperature using a TSL system (Mahwak, NJ). A confocal scanning laser microscope (CSLM) equipped with a gold-plated high-temperature furnace was used for real-time imaging of oxide growth on the sample surface. The specimens were heated in argon to approximately 620 or 720 °C at 10 °C/s and held. Both temperatures used were within the ferrite regimen of the sample material. This was confirmed during the experiment by the fact that the surface relief patterns caused by phase transformation were not observed (at temperatures above 750 °C they did appear). The pO_2 in the inlet and outlet gasses was measured to $10^{-4.8}$. CSLM combines confocal optics and helium-neon laser illumination to make possible observation of samples at high resolution at elevated temperatures. The process has been described in detail in the literature previously.[10] Confocal optics enables the detection of a strong signal from the focal plane while decreasing the intensity of signals not in the focal plane. Thus, the contrast on the surface topography is enhanced. The utilization of a laser results in high illumination intensity compared with the thermal radiation.

3. Results

3.1 Image Analysis

Typical CSLM images of the surface of an oxidizing specimen can be seen in Fig. 2(a), 4, 5, and 6(b). To interpret the developments that are shown in the images properly, an understanding of image formation in the CSLM is required. The CSLM makes use of the same optics and the same optical principles as a light optical microscope (LOM), but there are differences in the way contrast is formed. The more coherent laser light used in the CSLM allows an accurate discrimination of reflected light. To this end, a plate with a pinhole is placed in front of the detector,

which only allows light reflected from planes very close to the focal plane to pass and be detected. Light reflected from points on the specimen surface not in the focal place is excluded from the images, and such points appear black in the images, as opposed to LOM, where objects away from the focal plane become increasingly diffuse. The resolution of this discrimination of reflected light is approximately 100 nm. The advantage of this method of contrast formation is that it becomes easy to observe the evolution of oxides that form as particles on the specimen surface. However, attention must be paid, as can be seen from a comparison between Fig. 2(a) and (b). The figure shows a CSLM (Fig. 2a) and a scanning electron (SEM) micrograph (Fig. 2b) of the same area of a Mn/Al TRIP steel specimen oxidized under the above conditions. In Fig. 2(a), all of the boundaries appear dark compared with the grain interior, suggesting that a ridge of oxides exists along all boundaries, higher from the sample surface than the individual oxides in the grain interior surfaces. Comparison with Fig. 2(b) shows that this is not the case. Some of the boundaries that appear dark in the CSLM image have no oxide ridges along them, and indeed they seem less oxidized that the bounding grain interior surfaces.

With the surrounding grain surfaces oxidized, the not-oxidized grain boundaries form a relative valley and, with the focal plane of the CSLM positioned to maximize reflection from the surface as a whole, they appear dark. The accurate relationship between surface topography and image contrast may be exploited to distinguish between grain boundaries with oxide ridges and those without. Figure 2(c) shows a digitally binarized version of Fig. 2(a). By choosing the correct brightness discriminator, only the grain boundaries show which can be identified as having oxide ridges in Fig. 2(b). This method allows a faster way to identify oxidized grain boundaries and has been used in obtaining the observations below in all cases where there was ambiguity. Comparison of Fig. 2(a), (b), and (c) further yields the observation that the topographical resolution is much greater in the CSLM images (Fig. 2a) compared with the SEM images (Fig. 2b). In the SEM images, the difference in oxide particle height from the substrate between the oxide ridges on the grain boundaries and the oxide particles in the grain interior surfaces is not well observable, whereas this difference stands out clearly in Fig. 2(a) and (c).

3.2 Auger Electron Mapping

Auger electron maps of the surface chemistry of a typical (fine) grain are provided in Fig. 3 along with a SEM secondary electron micrograph of the same area (Fig. 3a).

The elements Mn, Fe, Al, and O are mapped in Fig. 3(b) to (e). The maps suggest a heterogeneous distribution of oxides across the specimen surface with Mn oxides forming oxide ridges on the grain boundaries and iron oxides forming individual particles on the grain interior surfaces. An area of grain boundary in Fig. 3(a) shows a high concentration of manganese, although there is no oxide ridge observed on that part of the grain boundary, suggesting that the formation of manganese oxide ridges is preceded by an increase of Mn in the grain boundary or that the conditions

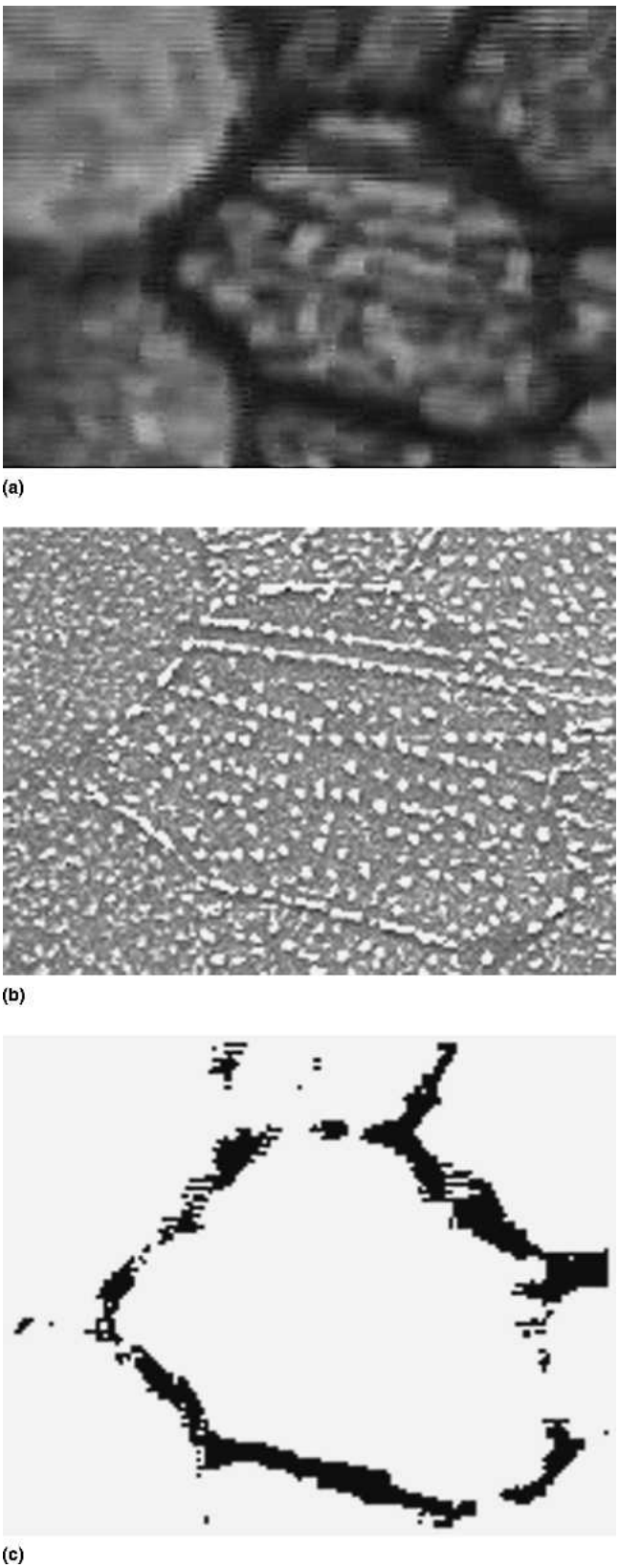

Fig. 2 (a) CSLM image of a coarse grained sample oxidized at 720 °C, (b) SEM SE image of the area shown in (a), and (c) Binarized version of (a)

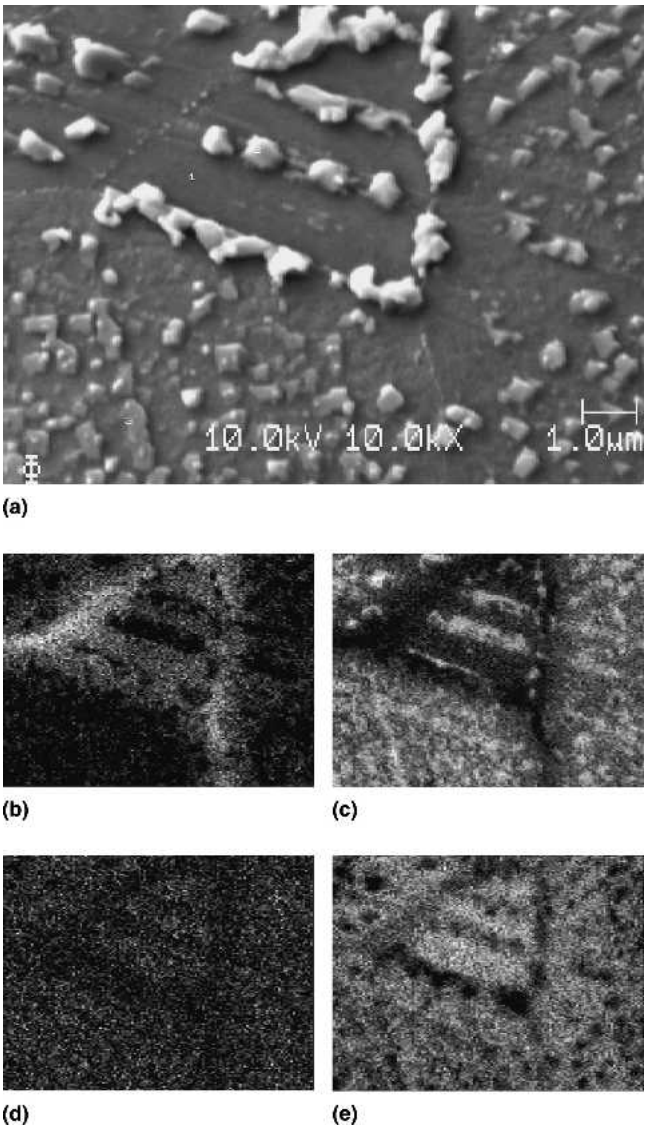

Fig. 3 Auger electron maps of element distribution on the surface of a coarse grained sample oxidized at 720 °C. (a) SEM SE image, (b) Mn, (c) Fe, (d) Al, and (e) O

allow internal oxidation of manganese at that part of the boundary. A fairly uniform distribution of Al across the surface suggests that none of the discrete particles on the specimen surface is an Al-rich compound, but the relative weakness of the O signal in areas with high Mn or Fe would suggest that Al has formed an oxide, either internally or as a homogeneous layer below the particles of Mn oxides and Fe oxides.

3.3 Effect of Temperature

Figure 4(a) to (c) shows CSLM images at 5 s intervals of a coarse-grained sample oxidizing at approximately 720 °C. The formation of oxide ridges is observed at all grain boundaries, but obvious differences are observed in the kinetics and to some degree in the morphological development between the boundaries. In the first image (Fig. 4a), no coherent oxide ridges are observed. In the second image (Fig. 4b) detectable oxides appear on many, but not all, boundaries. Figure 4(b) shows how the oxides form on the boundaries as individual particles first, and a comparison of Fig. 4(b) and (c) shows the morphological development of grain boundary oxides from individual particles dressing the boundaries, then coalescing to form the coherent ridges observed in Fig. 4(c).

In Fig. 4(c), coherent ridges have not formed on all boundaries, with some boundaries showing individual oxide particles.

Figure 4(d) to (f) shows CSLM images at 50 s intervals of a coarse-grained sample oxidizing at approximately 620 °C. The overall kinetics of oxidation is observed to be slower than that observed in Fig. 4(a) to (c), as might be expected. The morphological development of grain boundary oxidation observed in Fig. 4(d) to (f) is similar to that observed in Fig. 4(a) to (c) with oxidation starting at boundaries as discrete particles, which coalesce into coherent ridges. A marked difference between the behavior observed in Fig. 4(a) to (c) and that observed in Fig. 4(d) to (f) is that in the latter, many boundaries are not dressed with oxides. Figure 6(c) shows a binarized version of Fig. 4(f), allowing easy identification of boundaries with oxides.

3.4 Effect of Grain Size

Figure 5(a) to (c) shows CSLM images at 10 s intervals of a cold-rolled, fine-grained sample oxidizing at 720 °C. The oxide development at the grain boundaries is markedly different in these images compared with that observed for the coarse-grained samples above. Although the development of oxides at the grain boundaries still appears in the form of particle growth and coalescence, only a few boundaries show rich oxidation. The relative kinetics of oxidation at grain boundaries vs grain interior surfaces is also different from that observed in Fig. 3 and 4. In Fig. 4, oxides appear at grain boundaries relatively late compared with oxides at the grain interior surfaces.

X-ray diffraction (XRD) analysis of fine-grained specimens oxidized under the above conditions showed no presence of iron oxides, but marked peaks for MnO and Al_2O_3 were observed.

3.5 Correlation between Grain Boundary Oxidation and Grain Boundary Misorientation

Figure 6(a) shows a map of grain boundary misorientations in the specimen presented in Fig. 4(d) to (f). Figure 6(b) and (c) shows CSLM still and corresponding binarized images. No clear tendency can be derived from a correlation between the misorientation angle of a grain boundary and the oxidation at that boundary, except that no low-angle boundaries (<15°) have oxide ridges forming at their intersection with the specimen surface.

4. Discussion

The images in this paper provide in situ observation of the relative roles of selective oxidation through grain boundary diffusion and grain surface interior oxidation and

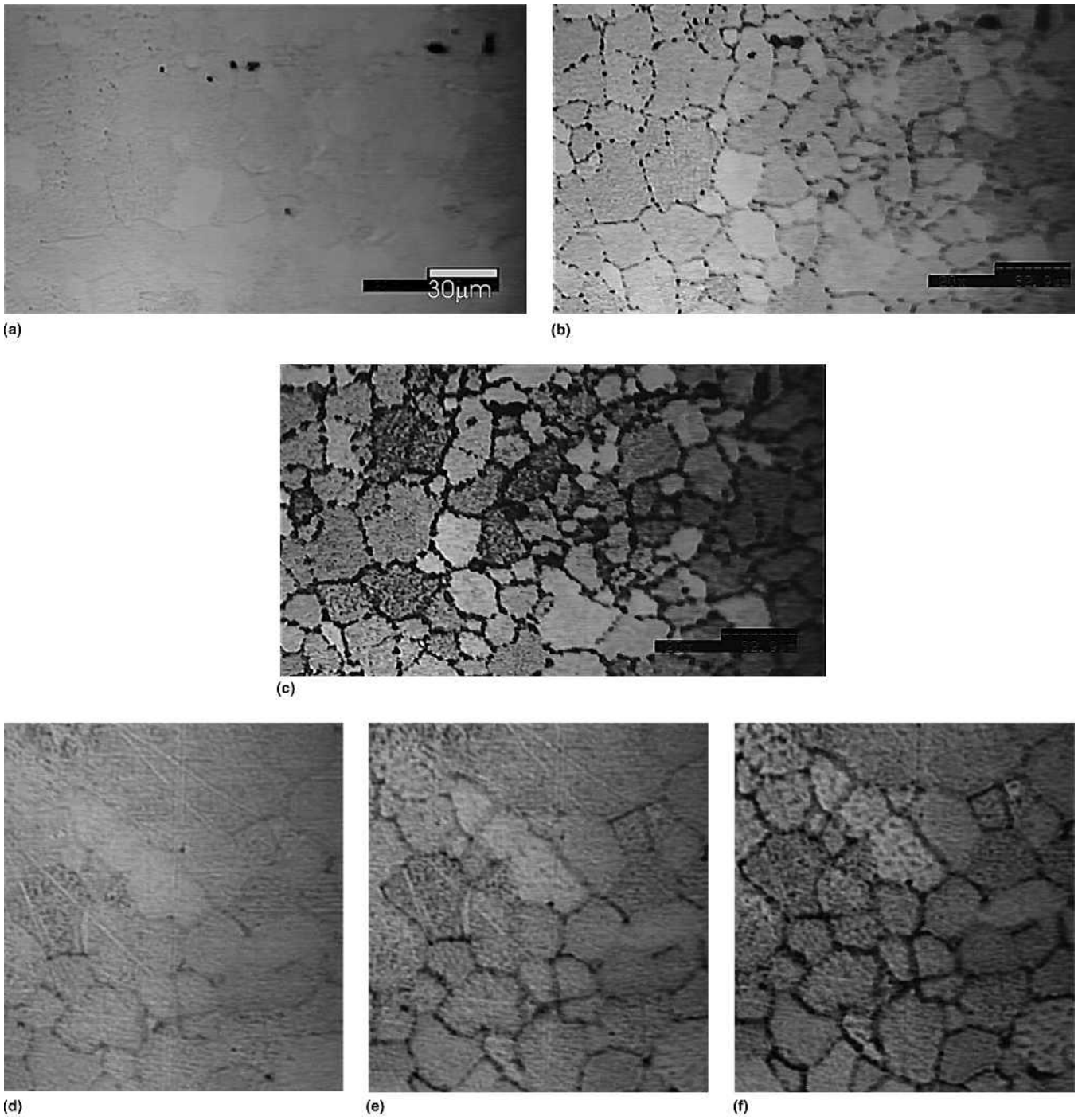

Fig. 4 (a) to (c) show a coarse grained sample oxidizing at approximately 720 °C, captured at 5 s intervals. (d) to (f) show a coarse grained sample oxidizing at approximately 620 °C, captured at 50 s intervals.

may in a broad sense confirm the mechanisms that have been proposed in literature.[2-8]

The overall kinetics and morphological development of surface oxides appear heavily influenced by the grain boundary diffusion of solute elements to the alloy surface. A mechanism as illustrated in Fig. 7 may be derived from the observations in Fig. 4. Manganese is brought to the surface almost exclusively through the grain boundaries, forming ridges of Mn oxides along the grain boundaries. Aluminum oxidizes internally, leaving the alloy surface free for iron oxides to be formed.

Changing the grain size of a sample seems to have a pronounced effect, not only on the morphological distribution of the oxides, which would be expected if the mechanism in Fig. 5 was repeated for a smaller grain size, but also the chemistry of the oxide products that are formed in the

(a)

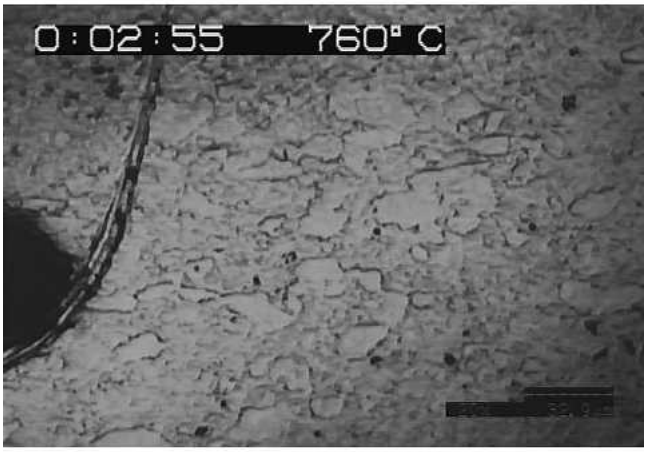

(b)

(c)

Fig. 5 Fine grained specimen oxidizing at 720 °C

fine-grained alloy is different from that in the coarse-grained alloy, with no Fe oxides formed in the fine-grained one. Alternative explanations can be offered for this observation. Close inspection of Fig. 5 reveals a pattern of oxidation in which ridges of Mn oxide enclose grains with entirely unoxidized surfaces. This suggests that a local equilibrium is established at the surface by the reaction of Mn and O. Because of the short distance between grain boundaries intersecting the surface in the fine-grained sample, no place on the specimen surface is far enough removed from the reaction of Mn and O not to be affected by the local equilibrium. Thus, Fe oxides cannot form on the surface. The portions of the surface which show some effect of oxidation outside the grain boundary ridges, may be Mn oxides appearing at the surface by diffusion through the lattice or dislocation pipes. However, a mechanism of local equilibrium would suggest that a similar absence of Fe oxides could be observed on the coarse-grained specimens in Fig. 4, at least within a distance from the grain boundary oxide ridges corresponding to half the grain diameter in the fine-grained specimen. But no such Fe oxide-depleted zone is observed in Fig. 4. Further, Fig. 6 shows no diffusion of Mn to the surface through low-angle grain boundaries, which makes it unlikely that Mn oxides can account for the oxidation observed at grain interior surfaces in Fig. 3 and 4. An alternative explanation would be that the much increased grain boundary area in the fine-grained sample compared with the coarse-grained sample changes the balance of internal and external oxidation for Al_2O_3, promoting external oxidation of Al according to Eq 1. In this case the formation of Al oxide on the sample surface would prohibit the formation of Fe oxide.

Increasing the temperature of oxidation of the coarse-grained sample results in an increase in the number of boundaries exhibiting oxidation. At 620 °C, the formation of Mn oxide ridges is absent at many boundaries. Although this is not the case at 720 °C, a marked difference is observed between boundaries in the kinetics of Mn oxide ridge formation. This strongly suggests a correlation between grain boundary crystallography and grain boundary diffusivity in accordance with observations by other investigators.[9] Figure 6 demonstrates that one parameter of the grain boundary, the misorientation, is not enough to investigate the nature of such a correlation in the random boundaries present in these specimens, in contrast to the pure-twist or pure-tilt boundaries investigated in the past. We therefore propose an expansion of the current method of combined EBSD mapping and CSLM observation to include serial sectioning as described by Randle[11] to characterize the grain boundaries fully. Removal of a layer of well-defined thickness parallel to the sample surface allows tracking of individual grain boundaries and the identification of the grain boundary inclination to the sample surface. Combined with identification of crystal orientation by EBSD, the full five parameters of the grain boundaries may be extracted. Subsequent observation of oxidation through CSLM, as above, is expected to enable correlation between grain boundary crystallography and grain boundary diffusivity. A similar approach has been applied successfully in the past to the study of wetting of grain boundaries in iron with copper.[12] One shortcoming in such an approach could be that it does not take the boundaries below those observed at the surface into account. The amount of Mn-containing oxide observed as ridges at grain boundaries in the above figures suggests a supply of Mn stemming from a depth below the surface greater than the grain size. Thus, the geography of grain boundaries below those observed at the surface could

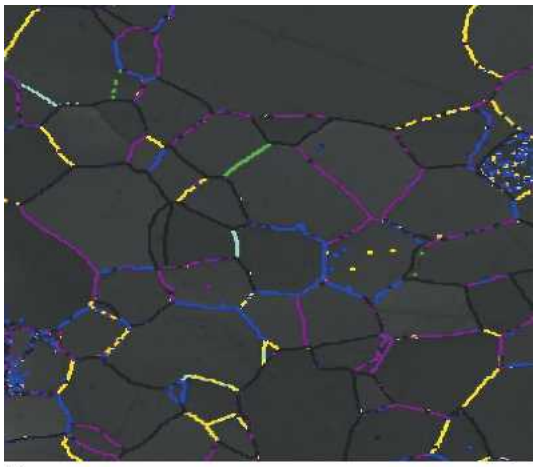

(a)

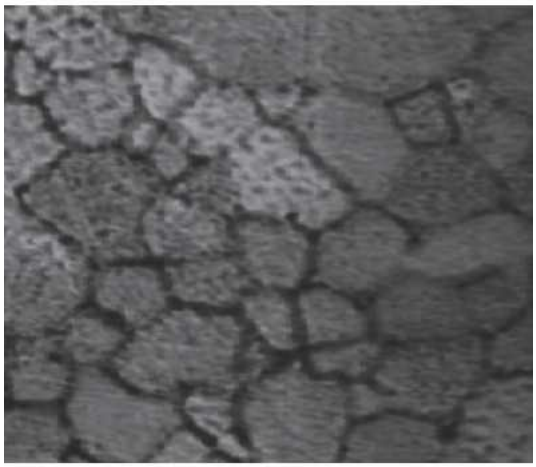

(b)

(c)

Fig. 6 (a) Shows grain boundaries colored according to the misorientation that they represent in the following intervals: 5-50° green, 10-15° turquoise, 15-20° orange, 20-30° blue, 40-50° violet, and 50-62.5° black; (b) shows a CSLM micrograph of the TRIP steel during oxidation at 620 °C; and (c) shows a Binarized version of (b), allowing easy identification of boundaries with oxides

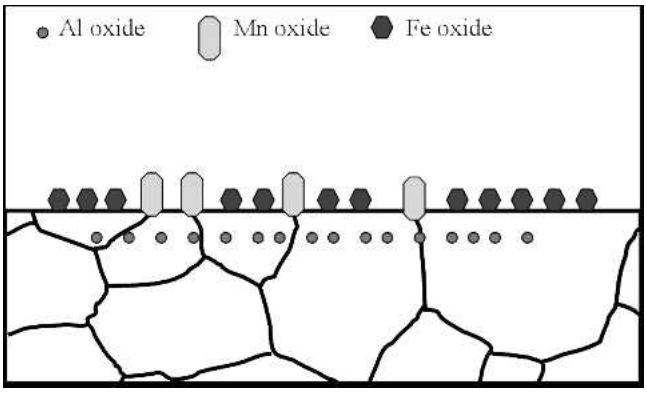

Fig. 7 Schematic of possible morphology

be limiting the diffusion of Mn to the observed boundaries, making direct correlation between grain boundary character and oxidation kinetics impossible.

5. Conclusions

The oxidation of AL-rich TRIP steel was investigated and the results suggest that:

- Al_2O_3 forms internally, whereas Mn and Fe oxides form on the sample surface.
- Mn oxides form preferentially at certain grain boundaries as a result of rapid diffusion. Low-angle boundaries appear to be less oxidized, especially at lower temperatures. No apparent correlation was found between grain boundary misorientation and oxidation kinetics for high-angle boundaries.
- Grain boundary oxidation precipitates as discrete particles, which coalesce into coherent ridges.
- Fe oxides tend to form at grain interiors but to a lesser degree at a smaller grain size.

Acknowledgment

The research presented in this paper was supported by National Science Foundation Grant DMR-0307188.

References

1. N. Birks and G.H. Meier, *Introduction to High-Temperature Oxidation of Metals,* Edward Arnold Ltd., London, 1983
2. J.G. Goedjen and D.A. Shores, Effect of Alloy Grain Size on the Transient Oxidation Behavior of an Alumina-Forming Alloy, *Oxidation Metals,* Vol 37 (No. 3-4), 1992, p 125-142
3. M.D. Merz, Oxidation Resistance of Fine-Grained Sputter-Deposited 304 Stainless Steel, *Metall. Trans. A,* Vol 10, 1979, p 71-77
4. M.K. Hossian, Effects of Grain Size on the High-Temperature Oxidation of an Fe-10% Cr Alloy, *Corr. Sci.,* Vol 19, 1979, p 1031-1045
5. R.K. Singh Raman et al., Influence of Grain Size on the Oxidation Resistance in 2¼Cr-1Mo Steel, *Oxidation Metals,* Vol 37 (No. 1-2), 1992, p 1-12
6. D.R. Baer and M.D. Merz, Differences in Oxides on Large- and Small-Grained Stainless Steel, *Metall. Trans. A,* Vol 11, 1980, p 1973-1980

7. D. Caplan and M. Cohen, Scaling of Iron at 500 °C, *Corr. Sci.,* Vol 3, 1963, p 139-143
8. J.M. Mataigne et al., Selective Oxidation of Cold-Rolled Steel during Recrystallization Annealing, *Developments in the Annealing of Sheet Steels,* R. Pradhan and I. Gupta, Ed., (TMS, Warrendale, PA, 1991)
9. A.P. Sutton and R.W. Balluffi, *Interfaces in Crystalline Materials,* Oxford University Press, 1995
10. S. Sridhar, P.D. Lee, and P. Rockett, Experimental Techniques for In Situ Characterization of Evolving Solidification Microstructures, *AFS Trans.,* Vol 110, 2002, p 147-158
11. V. Randle, Crystallographic Characterization of Planes in the Scanning Electron Microscope, *Mater. Char.,* Vol 34 (No. 1), 1995, p 29-34
12. M. Takashami et al., Correlation of Grain Boundary Character with Wetting Behavior, *Interface Sci.,* Vol 8, 2000, p 351-361